59Co and 6,7Li MAS NMR in polytypes O2 and O3 of LiCoO2

ARTICLE *in* THE JOURNAL OF PHYSICAL CHEMISTRY B · MAY 2001

Impact Factor: 3.3 · DOI: 10.1021/jp003832s

^{59}Co and ^{6,7}Li MAS NMR in Polytypes O2 and O3 of $LiCoO_2$

Renée Siegel and Jérôme Hirschinger*

Institut de Chimie, UMR 7510 CNRS, Bruker S.A., Université Louis Pasteur, BP 296, 67008 Strasbourg Cedex, France

Dany Carlier, Samir Matar, Michel Ménétrier, and Claude Delmas

Institut de Chimie de la Matière Condensée de Bordeaux - CNRS UPR 9048 and Ecole Nationale Supérieure de Chimie et Physique de Bordeaux, Château Brivazac, 162 Av. du Docteur A. Schweitzer, 33608 Pessac Cedex, France

Received: October 18, 2000; In Final Form: February 15, 2001

^{59}Co and ^{6,7}Li MAS NMR has been applied to polytypes O2 and O3 of $LiCoO_2$ at three different magnetic field strengths (4.7, 7.1, and 11.7 T). The ^{59}Co and ^{6,7}Li quadrupole and anisotropic shift tensors have been determined by iterative fitting of the NMR line shapes at the three magnetic field strengths. The magnitude of the quadrupole coupling constant at the cobalt site is about 3 times as large for the O2 variety as that for the O3 one. In ^{6,7}Li NMR, the ^{6,7}Li−^{6,7}Li and ^{6,7}Li−^{59}Co nuclear dipolar interactions had to be taken into account for a correct determination of the multiple interactions acting on the lithium nuclei. This was conveniently done by using a memory function approach. Calculations of the shift and quadrupole coupling parameters have been performed by using a point dipole and point monopole model, respectively. The shift tensor calculation shows that the magnetic susceptibility in both the O2 and O3 phases is due to Van Vleck paramagnetism for Co^{3+}. In the approximation of an ionic crystal, the electric field gradient (EFG) calculation leads to identical point charges at the atomic sites for the two varieties of $LiCoO_2$, and the observed difference in the quadrupole coupling constants results entirely from the fact that the CoO_6 octahedra share one face and three edges with the LiO_6 octahedra in the O2 phase and six edges in the O3 phase. However, our first-principles EFG calculations using the linearized-augmented-plane-wave (LAPW) method were only in qualitative agreement with the experimental data.

I. Introduction

$LiCoO_2$ is one of the leading positive electrode materials for secondary lithium batteries. The high-temperature phase of $LiCoO_2$ (noted O3) crystallizes in the rhomboedral system (space group $R\bar{3}m$) with the ideal layered α-$NaFeO_2$-type structure, the Li^+ and Co^{3+} ions occupying alternate layers of octahedral sites in the (111) planes (Figure 1).[1] This layered structure, which can be described as an ordered rock salt structure, has only one crystallographic site for the lithium and cobalt atoms. In 1982, Delmas et al.[2] synthesized a metastable variety of $LiCoO_2$ by Na/Li exchange from the layered precursor $Na_{0.70}CoO_2$. The structure of this material (noted O2) exhibits an unusual stacking of the oxygen layers where the LiO_6 and CoO_6 octahedra share not only edges as in the classical phase O3 but also faces (Figure 1). A first study of the electrochemical properties of this material in lithium batteries was reported by the same research group.[3] Very recently, the behavior of $LiCoO_2$(O2) was revisited in detail by Paulsen and Dahn,[4] who showed that the electrochemical properties are comparable to those of $LiCoO_2$(O3), although the two phases are different. Simultaneously, some of us undertook a general characterization of the structure and physical properties of the pristine and lithium-deintercalated phases (Li_xCoO_2(O2)), which will be published elsewhere.

* Corresponding author. Fax: +33 3 90 24 14 90. E-mail: hirschinger@chimie.u-strasbg.fr.

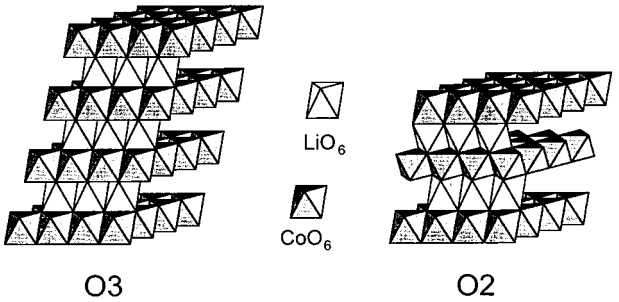

Figure 1. Schematic view of the structures O3 and O2 of $LiCoO_2$

Li_xCoO_2(O3) has been the subject of extensive electrochemical and X-ray studies,[1,5] showing the 2D character of these materials (absence of cobalt in lithium site), in contrast to the case of $LiNiO_2$. Solid-state NMR spectroscopy, which is a complementary technique for characterizing the structure at the length scale of the chemical bond,[6] has also been applied in Li_xCoO_2 (x denotes the Li/Co ratio of the starting mixture) to observe small departure from stoichiometry as well as the phase changes upon lithium deintercalation.[7−14] Indeed, ^{7}Li magic-angle-spinning (MAS) NMR spectra of compounds with Li/Co ratios slightly higher than 1 ($x > 1$) exhibit new signals which have been attributed to paramagnetic low-spin Co^{2+} ions.[11,14] On the other hand, for slightly deintercalated materials ($0.94 < x < 1$), localized Co^{4+} ions lead to a partial loss of observability of the ^{7}Li NMR signal, owing to a very strong directly transferred hyperfine interaction between the unpaired electron

10.1021/jp003832s CCC: $20.00
Published on Web 04/21/2001

in a t_2 orbital and the first lithium neighbors, while for higher deintercalation amounts ($x < 0.94$), a new signal attributed to a metallic phase is observed.[12,14] ^{59}Co NMR has also been applied successfully to Li_xCoO_2(O3), thus demonstrating that the cobalt ions are in a low-spin trivalent state (LS t_2^6).[10,11] Complicating these NMR measurements is the fact that the ^{59}Co nucleus ($I = 7/2$) has a rather large quadrupole moment ($Q = 0.42 \times 10^{-24}$ cm^2). This is probably the reason only a few polycrystalline diamagnetic complexes and clusters have been studied by ^{59}Co NMR.[15−17] In agreement with the ^{7}Li NMR results, the ^{59}Co MAS spectra show evidence for the presence of several cobalt sites in Li_xCoO_2(O3), depending on the Li/Co ratio ($x > 0.95$).[11] However, to our knowledge, no attempts have been made to determine the multiple interaction tensors such as the electric field gradient (EFG) or quadrupolar (**Q**) tensor, the shift anisotropy (**S**) tensor, and the nuclear dipolar couplings acting on the ^{59}Co, ^{6}Li and ^{7}Li nuclei in $LiCoO_2$. These interactions are of primary importance since they may be directly related to the structure of the different polytypes. Indeed, in such ionic crystals, the quadrupolar tensors may be used to test several atomic charges distributions, while the shift tensors depend on the magnetic properties of these materials.[18,19]

In the present paper, we use ^{59}Co, ^{6}Li, and ^{7}Li MAS NMR in order to characterize the structure of polytypes O2 and O3 of $LiCoO_2$. The experimental quadrupole and shift coupling parameters are compared with calculations using a point monopole and point dipole model, respectively. A first-principles calculation of the EFG parameters at the cobalt and lithium sites using the full-potential linearized augmented plane wave (FP-LAPW) method based on density functional theory (DFT) is also attempted, and comparison with the experimental data is described and discussed.

II. Experimental Section

A. Sample Preparation. *$LiCoO_2$(O3).* The O3 variety of $LiCoO_2$ (stoichiometric sample) was prepared from a mixture of Li_2CO_3 (Rhône-Poulenc Rectapur, 99% min) and Co_3O_4 (calcination at 450 °C for 12 h under O_2 of $Co(NO_3)_2 \cdot 6H_2O$ Carlo Erba, 99% min). The stoichiometric mixture was ground, pelletized, and treated at 600 °C for 12 h under O_2 and twice at 900 °C for 24 h with intermediate grinding.

$LiCoO_2$(O2). The metastable O2 variety of $LiCoO_2$ was obtained by ion exchange reaction from the $Na_{0.7}CoO_2$ starting material. This starting material was prepared by solid-state reaction of a mixture of Na_2O (Aldrich, 99% min) and Co_3O_4 at 800 °C for 48 h under O_2. 5% Na_2O excess was used to compensate for evaporation. The starting mixture was ground and pelletized in a drybox (under argon), and the final material was quenched into liquid nitrogen. The exchange reaction was carried out as described in ref 2, using an LiCl solution in methanol (5 M). The exchange was performed several times over 3 weeks, with intermediate washing, drying and grinding. A very small amount of the sodium precursor still remains after the last exchange.

B. NMR Measurements. ^{59}Co, ^{6}Li, and ^{7}Li NMR measurements were carried out at room temperature on Bruker ASX-200 ($B_0 = 4.7$ T, Larmor frequency $\nu_0 = 48.1$, 29.4, and 77.8 MHz in ^{59}Co, ^{6}Li, and ^{7}Li resonance, respectively), Bruker MSL-300 ($B_0 = 7.1$ T, $\nu_0 = 71.2$, 44.2, and 116.6 MHz in ^{59}Co, ^{6}Li, and ^{7}Li resonance, respectively), and Bruker Avance DSX-500 ($B_0 = 11.7$ T, $\nu_0 = 120.4$, 73.6, and 194.3 MHz in ^{59}Co, ^{6}Li, and ^{7}Li resonance, respectively) spectrometers. Single-pulse MAS spectra were obtained by using a Bruker MAS probe with a cylindrical 4-mm o.d. rotor. Spinning frequencies ν_r up to 15 kHz were utilized. In ^{59}Co experiments, a short pulse length of 1 μs corresponding to a nonselective $\pi/12$ pulse determined using an aqueous solution of $K_3[Co(CN)_6]$ salt was employed. In ^{6}Li and ^{7}Li experiments, pulse lengths of about 5 μs corresponding to a pulse angle close to 90° were used. Recycle times were ∼1, ∼100, and ∼3 s in ^{59}Co, ^{6}Li, and ^{7}Li resonance, respectively. The baseline distortions resulting from the spectrometer deadtime (5−10 μs) were removed computationally using a polynomial baseline correction routine. The isotropic shifts, reported in parts per million, are relative to an external sample of $K_3[Co(CN)_6]$ (^{59}Co NMR) or LiCl (^{6,7}Li NMR) in H_2O.

The ^{59}Co and ^{6,7}Li MAS NMR spectra were simulated directly in the frequency domain as described previously.[18,19] No finite pulse length correction was included in the simulation. This is usually an acceptable approximation considering the short pulses employed. The NMR parameters were determined by nonlinear least-squares fitting of the experimental integrated spinning sideband (ssb) intensities I_N^{exp} using Powell's method[20] from the numerical recipes package.[21] Subsequently, the accuracy of each parameter was obtained by the postoptimal analysis for nonlinear least-squares fitting performed by the subroutine SV02A of the Harwell subroutine library. To account for the nuclear dipole−dipole interactions, we also fitted the ^{6,7}Li MAS NMR spectra using a memory function approach as described in section III. B.

III. Results and Discussion

The structural parameters used in the following for the calculations were obtained by the Rietveld refinement of X-ray diffraction spectra of the O2 and O3 phases:
$LiCoO_2$(O2): s.g.; $P6_3mc$; $a = 2.803$ Å; $c = 9.538$ Å; O1(2a), (0,0,0.11); O2(2b), ($^1/_3$,$^2/_3$,0.39); Li(2b), ($^1/_3$,$^2/_3$,0.75); Co(2b), ($^1/_3$,$^2/_3$,1)
$LiCoO_2$(O3)[12]: s.g.; $R\bar{3}m$; $a = 2.816$ Å; $c = 14.049$ Å; O(6c), (0,0,0.7397); Li(3b), (0,0,0.5); Co(3a), (0,0,0).

A. ^{59}Co NMR. Figures 2 and 3 show the experimental ^{59}Co MAS NMR spectra of polytypes O2 and O3, respectively, of $LiCoO_2$ at the three available magnetic field strengths. The MAS spectra are observed to break up into spinning sidebands (ssb's), in agreement with previous ^{59}Co NMR measurements on $LiCoO_2$(O3).[10,11] In $LiCoO_2$(O2), all ssb's are quite well described by Lorentzian−Gaussian lines, with a constant full-width at half-height (fwhh) of ∼4 kHz, whereas the fwhh is observed to increase strongly with B_0 in the O3 phase (from ∼1.8 kHz at 4.7 T to ∼3 kHz at 11.7 T). For simplicity, in Figures 2 and 3, the isotropic peak, determined from spectra employing different spinning speeds, was arbitrarily chosen as the chemical shift reference. The observation of a single isotropic peak for both polytypes, at 13815 ± 5 ppm for the phase O2 and at 14115 ± 5 ppm for the phase O3, is consistent with the presence of only one crystallographic site for the cobalt atoms (Figure 1), and the absence of significant quadrupolar second-order shifts indicates that the quadrupole coupling constant $Q_{CC} = e^2qQ/h$ is moderate ($|Q_{CC}| < 5$ MHz). Indeed, the good agreement between the experimental and calculated data (Figures 2 and 3) demonstrates that the complete manifolds of ssb's from all seven ^{59}Co transitions are detected. As previously noted,[10,11] the asymmetric manifolds of ssb's show the presence of a large chemical shift anisotropy. Since the isotropic shift and the linebroadening need not be included in the optimization, the fit of the ssb intensities yields in principle the following seven parameters: the shift (S) anisotropy δ_S and its asymmetry

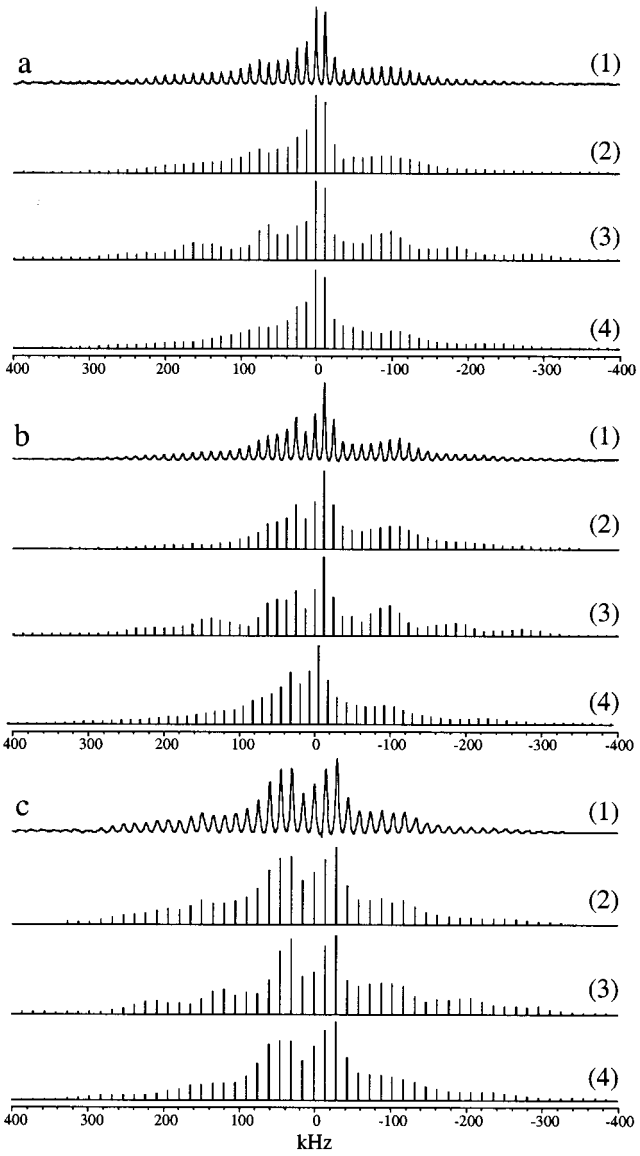

Figure 2. Experimental and fitted ^{59}Co MAS NMR spectra of $LiCoO_2$-(O2): (a) 4.7 T, $\nu_r = 12.00$ kHz; (b) 7.1 T, $\nu_r = 12.46$ kHz; (c) 11.7 T, $\nu_r = 14.90$ kHz; (1) experimental spectrum; (2) stick plot of the integrated ssb intensities I_N^{exp} for the spectrum in (1) used in the fit; (3) stick plot of the calculated ssb intensities I_N^{calc} corresponding to the optimized parameters from the fitting procedure (Table 1) with coaxial and axially symmetric **S** and **Q** tensors (two-parameter fit); (4) stick plot of the calculated ssb intensities I_N^{calc} corresponding to the optimized parameters from the fitting procedure (Table 1) with noncoincident and asymmetric **S** and **Q** tensors (seven-parameter fit).

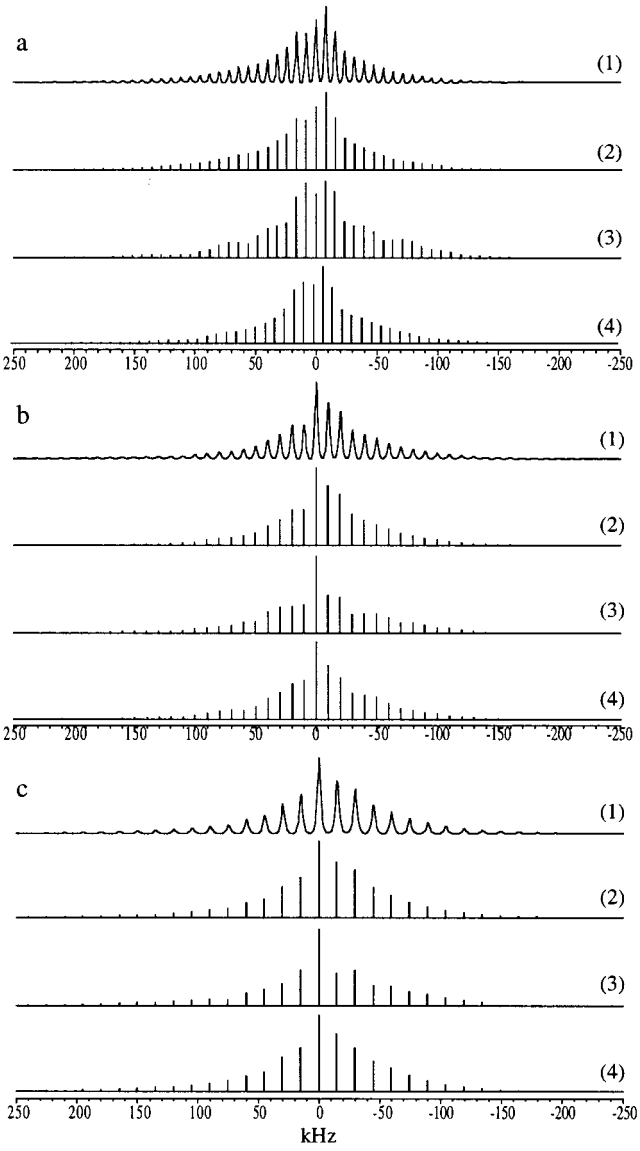

Figure 3. Experimental and fitted ^{59}Co MAS NMR spectra of $LiCoO_2$-(O3): (a) 4.7 T, $\nu_r = 6.25$ kHz;(b) 7.1 T, $\nu_r = 10.00$ kHz; (c) 11.7 T, $\nu_r = 15.06$ kHz; (1) experimental spectrum; (2) stick plot of the integrated ssb intensities I_N^{exp} for the spectrum in (1) used in the fit; (3) stick plot of the calculated ssb intensities I_N^{calc} corresponding to the optimized parameters from the fitting procedure (Table 1) with coaxial and axially symmetric **S** and **Q** tensors (two-parameter fit); (4) stick plot of the calculated ssb intensities I_N^{calc} corresponding to the optimized parameters from the fitting procedure (Table 1) with noncoincident and asymmetric **S** and **Q** tensors (seven-parameter fit).

parameter η_S, the absolute value of the quadrupole (Q) coupling constant $|Q_{CC}|$ and corresponding asymmetry parameter η_Q, and the Euler angles ψ, χ, ξ which transform the **S** tensor from its principal axes system (PAS) to the PAS of the **Q** tensor.[22,18] In our case, it is nevertheless useful to consider the crystallographic symmetry. Indeed, the presence of a 3-fold rotation symmetry at the cobalt site (along the *c* axis) in both structures O2 and O3 (Figure 1) implies that the **S** and **Q** tensors are coincident ($\psi = \chi = \xi = 0$) and axially symmetric ($\eta_S = \eta_Q = 0$). Figure 2 shows that the ^{59}Co MAS NMR results are in good agreement with these symmetry requirements in the case of $LiCoO_2$(O2), the corresponding two-parameter fit at the three available magnetic field strengths giving $\delta_S = 660 \pm 41$ ppm and $|Q_{CC}| = 2614 \pm 80$ kHz (Table 1). Moreover, no significant improvement of the fit is obtained when considering asymmetric and noncoincident **S** and **Q** tensors (seven-parameter fit), the slight intensity losses near the outer edges of the spectra (Figure

TABLE 1: Fitted Interaction Parameters for the ^{59}Co MAS NMR Spectra of the Phases O2 and O3 of $LiCoO_2$ at B_0 = 4.7, 7.1, and 11.7 T

	phaseO2		phaseO3	
interaction parameter	two-parameter fit	seven-parameter fit	two-parameter fit	seven-parameter fit
δ_S (ppm)	660 ± 41	647 ± 40	721 ± 47	689 ± 35
η_S	0	0.15 ± 0.15	0	0.2 ± 0.2
$\|Q_{CC}\|$ (kHz)	2614 ± 80	2387 ± 121	927 ± 47	822 ± 32
η_Q	0	0.4 ± 0.1	0	0.4 ± 0.1
ψ (deg)	0	-	0	-
χ (deg)	0	25 ± 15	0	9 ± 6
ξ (deg)	0	-	0	-

2) being attributed to line shape distortions resulting from the finite pulse length and/or the quality factor of the MAS probe.[23] This is a clear confirmation of the presence of a C_3 axis at the cobalt site in the structure O2 of $LiCoO_2$. The fact that the Euler angles ψ and ξ are found to be completely undetermined within our precision criteria (Harwell subroutine SV02A) is readily understood, recalling that the line shape becomes insensitive to the angle ψ or ξ as η_S or η_Q tends toward 0, respectively. On the other hand, in the case of $LiCoO_2$(O3), Figure 3 shows that a satisfactory description of the experiments is not achieved when assuming a C_3 symmetry at the cobalt site (two-parameter fit) and that a better agreement is obtained when considering asymmetric and noncoincident **S** and **Q** tensors (seven-parameter fit), although some discrepancies are still observed. These discrepancies are particularly obvious in the spectrum at low magnetic field ($B_0 = 4.7$ T) which exhibits most sidebands and, thus, should be the most sensitive to the interaction parameters. Note that line shape distortions resulting from the finite pulse length and/or the quality factor of the MAS probe cannot be invoked in the case of $LiCoO_2$(O3) since the envelopes of ssb intensities (Figure 3) then are very similar to the ones we have previously obtained in V_2O_5 by ^{51}V MAS NMR.[19] Moreover, the resulting asymmetry of the electric field gradient tensor at the cobalt site ($\eta_Q \approx 0.4$) cannot be reconciled with the symmetry requirements of the O3 structure ($\eta_Q = 0$). Using the memory function approach described below (section III.B), we have verified that the ^{59}Co−^{59}Co and ^{59}Co−^{6,7}Li nuclear dipolar interactions are too weak to contribute significantly to the ssb intensities of the spectra shown in Figure 3. Hence, in connection with recent observations,[10,11,14] the fact that our fitting procedure fails to describe the ^{59}Co NMR experiments in $LiCoO_2$(O3) may rather be attributed to the presence of some structural defects leading to an inhomogeneous distribution of the NMR interaction parameters. Indeed, Ganguly et al.[10] have suggested the existence of two cobalt signals with the same isotropic shift but with different anisotropic components, while Peeters et al.[11] have detected three overlapping spinning sideband manifolds in Li_xCoO_2(O3) with a Li/Co ratio higher than 0.95. As confirmed by the ^{6,7}Li NMR spectra shown in the following, the analyzed O3 sample does not present the structural defects which were attributed to a Li/Co ratio higher than 1, nor the consecutive presence of Co^{2+} ions and oxygen deficiency.[14] Furthermore, the ^{59}Co NMR spectra also exhibit a single resonance. However, one cannot exclude that the Li/Co ratio is very slightly lower than 1, so some localized Co^{4+} ions might be present. Indeed, this was shown to lead to the loss of NMR observation for some Li^+ ions but not to the presence of any additional ^{7}Li NMR signal.[12] In samples with an excess of lithium ($x > 1$), prepared as in ref 14, we have also observed an increase of the ssb line width (fwhh of ∼7 kHz at 11.7 T for $x = 1.1$) as well as of the shift anisotropy (data not shown). Hence, structural disorder may be present although the studied sample is in principle stoichiometric ($x = 1$) and exhibits single cobalt and lithium resonances. Note that the increase of the ssb line width with B_0 observed for the O3 phase (Figure 3) clearly supports the presence of unresolved cobalt signals whose spinning sideband manifold leads fortuitously to an asymmetric **Q** tensor. Since the values of δ_S and Q_{CC} derived from the two- and seven-parameter fits are similar (Table 1), it may nevertheless be concluded that the magnitude of these interaction parameters is essentially unaffected by the structural disorder evidenced in $LiCoO_2$(O3) and that polytype O2 is characterized by a quadrupole coupling constant about 3 times larger than that of polytype O3.

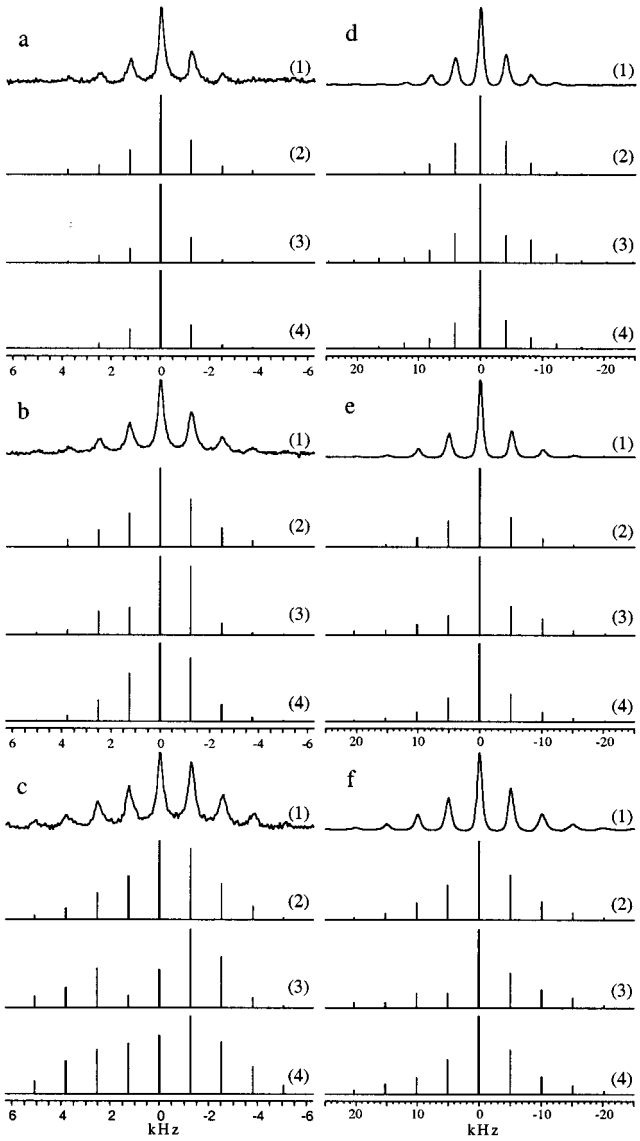

Figure 4. Experimental and fitted ^{6}Li and ^{7}Li MAS NMR spectra of $LiCoO_2$(O2): (a) ^{6}Li, 4.7 T, $\nu_r = 1.25$ kHz; (b) ^{6}Li, 7.1 T, $\nu_r = 1.26$ kHz; (c) ^{6}Li, 11.7 T, $\nu_r = 1.27$ kHz; (d) ^{7}Li, 4.7 T, $\nu_r = 4.10$ kHz; (e) ^{7}Li, 7.1 T, $\nu_r = 5.09$ kHz; (f) ^{7}Li, 11.7 T, $\nu_r = 5.07$ kHz; (1) experimental spectrum; (2) stick plot of the integrated ssb intensities I_N^{exp} for the spectrum in (1) used in the fit; (3) stick plot of the calculated ssb intensities I_N^{calc} corresponding to the optimized parameters from the fitting procedure (Table 2) with coaxial and axially symmetric **S** and **Q** tensors (two-parameter fit); (4) stick plot of the calculated ssb intensities I_N^{calc} corresponding to the optimized parameters from the fitting procedure (Table 2) with noncoincident and asymmetric **S** and **Q** tensors (seven-parameter fit)

B. ^{6,7}Li NMR. The ^{6}Li and ^{7}Li MAS NMR spectra of the O2 and O3 $LiCoO_2$ varieties are reported in Figures 4 and 5, respectively. As already mentioned, the experiments show only one lithium resonance centered at −0.2 ppm, in accordance with the presence of one lithium site octahedrally coordinated by oxygen (Figure 1). The line widths (fwhh) of the ^{6}Li and ^{7}Li resonances for both the O2 and O3 phases are approximately 0.3 kHz and 1 kHz, respectively. Moreover, in contrast to the ^{59}Co results (Figures 2 and 3), it is seen that the ^{6}Li and ^{7}Li ssb intensities of the O2 and O3 phases are very similar. Both the magnitudes and relative orientation of the **Q** and **S** tensors have been previously determined by iterative fitting of the ^{6}Li and ^{7}Li MAS NMR ssb intensities in a series of $Li_xV_2O_5$ bronzes,[18] the large difference between the ^{6}Li and ^{7}Li quadrupole moments

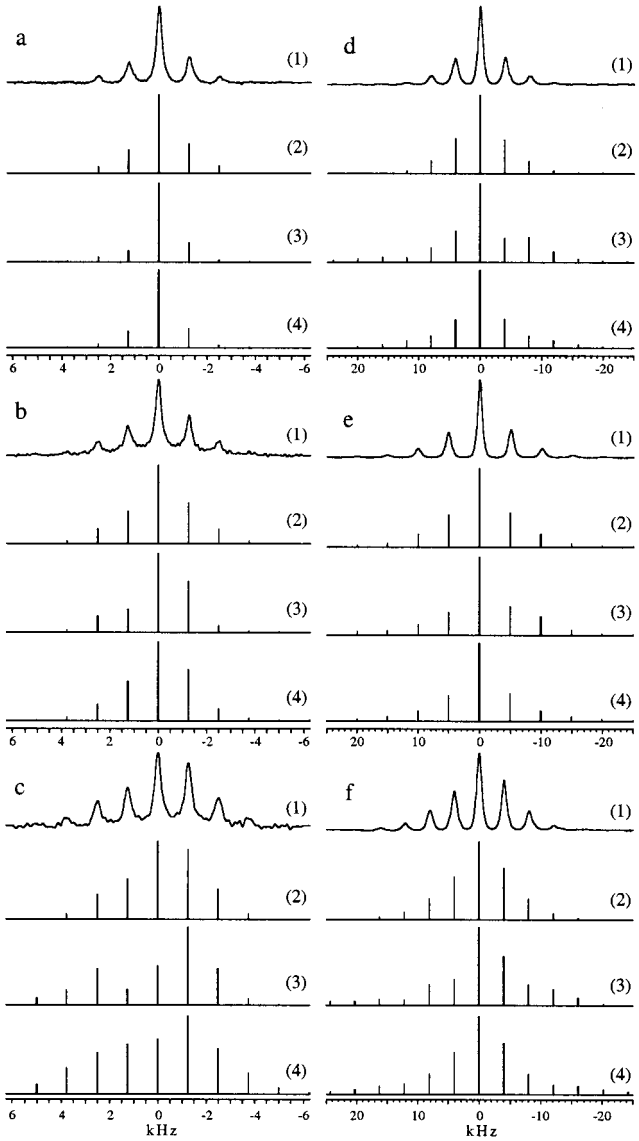

Figure 5. Experimental and fitted ^{6}Li and ^{7}Li MAS NMR spectra of $LiCoO_2$(O3): (a) ^{6}Li, 4.7 T, $\nu_r = 1.25$ kHz; (b) ^{6}Li, 7.1 T, $\nu_r = 1.25$ kHz; (c) ^{6}Li, 11.7 T, $\nu_r = 1.25$ kHz; (d) ^{7}Li, 4.7 T, $\nu_r = 4.00$ kHz; (e) ^{7}Li, 7.1 T, $\nu_r = 5.00$ kHz; (f) ^{7}Li, 11.7 T, $\nu_r = 4.06$ kHz; (1) experimental spectrum; (2) stick plot of the integrated ssb intensities I_N^{exp} for the spectrum in (1) used in the fit; (3) stick plot of the calculated ssb intensities I_N^{calc} corresponding to the optimized parameters from the fitting procedure (Table 2) with coaxial and axially symmetric **S** and **Q** tensors (two-parameter fit); (4) stick plot of the calculated ssb intensities I_N^{calc} corresponding to the optimized parameters from the fitting procedure (Table 2) with noncoincident and asymmetric **S** and **Q** tensors (seven-parameter fit)

($Q(^7Li)/Q(^6Li) \approx 56$) being particularly useful for an accurate determination of the NMR interaction parameters. Indeed, while the ^{7}Li NMR spectra are usually dominated by the quadrupolar interaction, an accurate determination of the shift interaction can be obtained in ^{6}Li resonance.[18,24] The same analysis has been performed here for polytypes O2 and O3 of $LiCoO_2$.

Figures 4 and 5 show that a good agreement between the experiment and calculation cannot be obtained by iterative fitting of the ^{6}Li and ^{7}Li MAS NMR line shapes at the three magnetic field strengths, especially when considering the C_3 symmetry at the lithium site (two-parameter fit). This is particularly obvious in ^{6}Li resonance at high magnetic field (Figures 4c and 5c). As expected, the resulting interaction parameters for polytypes O2 and O3 listed in Table 2 are equal within

TABLE 2: Fitted Interaction Parameters for the ^{6,7}Li MAS NMR Spectra of the Phases O2 and O3 of $LiCoO_2$ at B_0 = 4.7, 7.1, and 11.7 T

	phaseO2		phaseO3	
interaction parameter	two-parameter fit	seven-parameter fit	two-parameter fit	seven-parameter fit
δ_S (ppm)	77 ± 9	73 ± 8	68 ± 8	67 ± 8
η_S	0	0.75 ± 0.25	0	0.75 ± 0.25
$\lvert Q_{CC}(^7Li)\rvert$ (kHz)	36 ± 8	25 ± 12	39 ± 7	31 ± 14
η_Q	0	-	0	-
ψ (deg)	0	-	0	-
χ (deg)	0	25 ± 25	0	-
ξ (deg)	0	-	0	-

experimental accuracy. Note that the slight improvement of the fit obtained when considering asymmetric and noncoincident **CS** and **Q** tensors (seven-parameter fit) is found to be almost completely accounted for by an increase of η_S toward ~0.75 (Table 2). Furthermore, neither the small quadrupole coupling constant ($|Q_{CC}(^7Li)| \sim 30-40$ kHz) nor the relative orientation of the two interaction tensors can be determined accurately, and η_Q is found to be completely undetermined within our precision criteria (Table 2). Actually, as a consequence of the low $|Q_{CC}(^7Li)|$ value, the quadrupolar interaction does not contribute significantly to the ^{6}Li ssb intensities ($Q_{CC}(^7Li)/Q_{CC}(^6Li) \approx 56$). The fact that our fitting procedure fails to describe the ^{6}Li and ^{7}Li experiments may then be attributed to the effect of the ^{6,7}Li$-^{6,7}$Li and ^{6,7}Li$-^{59}$Co nuclear dipolar interactions. Indeed, close inspection of the ^{6}Li spectra of Figures 4 and 5 clearly supports the presence of an additional field-independent interaction and the observation of only a few wide-spinning sidebands points toward the homogeneous character of the multispin homonuclear dipolar Hamiltonian.[25] In retrospect, the fact that a perfect agreement with the experimental spectrum was not achieved in ^{6}Li resonance for the β phase of $Li_xV_2O_5$[18] may similarly be attributed to the effect of the ^{6,7}Li$-^{6,7}$Li and ^{6,7}Li$-^{51}$V nuclear dipolar couplings. It is well-known that the line shape calculation for a rigid assembly of spins coupled together by homonuclear dipolar interactions cannot be performed exactly.[26] The problem is even more complicated in the presence of MAS, when the Hamiltonians at various times do not commute with each other.[27,28] In the following, we shall then adopt a simple analytical method based on a stochastic theory involving a correlation function, the memory function, which describes the time-averaged fluctuations of the dipolar local field.[29] This memory function approach which allows to ignore the detailed structure of the spin system has been shown to provide good agreement with free induction decay and cross-polarization experimental data[30-32] in the Anderson−Weiss approximation limit.[29,31,33] To take into account both the quadrupolar, shift, and nuclear dipolar interactions, it is further possible to construct a system exhibiting intermediate characteristics by using the following product for the free induction decay:

$$G(t) = G_D(t) * \sum_N I_N^{calc} \exp(iN\omega_r t) \qquad (1)$$

where the I_N^{calc} are the ssb intensities for the **Q** and **S** interactions calculated as described previously[18,19] and $G_D(t)$ is the decay due to the nuclear dipolar interactions obtained by using the memory function approach[30,32]

$$G_D(t) = \exp\left\{M_2\left[\frac{2}{3}f(\Gamma,\omega_r,t) + \frac{1}{3}f(\Gamma,2\omega_r,t)\right]\right\} \qquad (2)$$

where

$$f(\Gamma,\omega_r,t) = \frac{1}{\Gamma^2 + \omega_r^2} \times \left\{ \frac{[(\Gamma^2 - \omega_r^2)(1 - \cos \omega_r t) + 2\Gamma\omega_r \sin \omega_r t] \exp(-\Gamma t)}{\Gamma^2 + \omega_r^2} - \Gamma t \right\}$$

and $\Gamma = 1/\tau_c$, where τ_c is the correlation time describing the stochastic process of the fluctuations of the expectation values for the z component of the spins due to flip-flop transitions. Note that these assumptions enable us to describe the whole of the dipolar interactions in terms of one parameter, M_2, the second moment of the resonance absorption line which can be calculated from the atomic positions of the crystal structure.[26] In other words, each spin is supposed to interact to a small degree with a large number of other spins so that the orientation dependence of the nuclear dipolar interactions may be neglected. This is expected to be the case for $LiCoO_2$ (Figure 1).

Figures 6 and 7 show the optimization of the ^{6}Li and ^{7}Li line shapes with the memory function approach. In contrast to the **Q**/**S** analysis presented above for which the Hamiltonian behaves inhomogeneously, i.e., the calculated MAS spectra are discrete sets of δ-functions (Figures 2−5), the broadening of the lines simulated by the memory function approach (Figures 6 and 7), which is reminiscent of the homogeneous character of the dipolar interactions, can also be optimized. The line width of the central line and of the sidebands decreases with increasing values of τ_c and ω_r. Since the second moment M_2 can be computed from the crystal structure, only the four parameters, δ_S, $|Q_{CC}(^7Li)|$, $\tau_c(^6Li)$, and $\tau_c(^7Li)$, need to be included in the optimization when considering the C_3 symmetry at the lithium site. Moreover, the contribution of the quadrupolar interaction being negligibly small in ^{6}Li resonance ($|Q_{CC}(^7Li)| \approx 30-40$ kHz), the ^{6}Li MAS spectra may be described by the two parameters, δ_S and $\tau_c(^6Li)$. Indeed, Figures 6 and 7 show that a good fit of the experiments at the three magnetic field strengths is obtained with $\delta_S = 47 \pm 3$ ppm for the O2 phase and with $\delta_S = 45 \pm 3$ ppm for the O3 phase. Note also that the consideration of the dipolar interactions results in a smaller shift anisotropy than obtained from the **Q**/**S** analysis ($\delta_S \approx 70$ ppm). Actually, our analysis demonstrates that the nuclear dipole−dipole interactions account for about 83% of the contribution to the simulated ^{6}Li ssb intensities at low field, $B_0 = 4.7$ T (Figures 6a and 7a). δ_S being fixed by the fit of the ^{6}Li data, the ^{7}Li MAS spectra have been subsequently simulated in Figures 6 and 7 for several $|Q_{CC}(^7Li)|$ values between 0 and 40 kHz. The fact that $\tau_c(^7Li)$ (∼0.3 ms) is much shorter than $\tau_c(^6Li)$ (∼1.2 ms) is not surprising since spin diffusion is expected to be driven by the energy-conserving flip-flop transitions of neighbor ^{7}Li−^{7}Li spin pairs. When ignoring the quadrupolar interaction ($|Q_{CC}(^7Li)| = 0$), it appears that the dipolar interactions give rise to ∼87% of the simulated ^{7}Li ssb intensities at $B_0 = 4.7$ T. These observations clearly show that the dipolar interactions must be considered in the analysis of both ^{6}Li and ^{7}Li MAS spectra in $LiCoO_2$. Moreover, considering the crudeness of the line shape calculation (eq 1), the ^{7}Li manifolds of ssb's at the three magnetic field strengths are found to be in reasonable agreement with the simulations for $|Q_{CC}(^7Li)|$ in the range of 30−40 kHz (Figures 6 and 7). Hence, although quadrupolar broadening is appreciable in ^{7}Li resonance, the quadrupole coupling constant is small for both polytypes O2 and O3, in agreement with the **Q**/**S** analysis (Table 2).

C. Point Dipole Calculation of the ^{6,7}Li Shift Coupling Parameters. Since the Co^{3+} ion in a low-spin state is diamagnetic (LS t_2^6), no hyperfine interaction is expected for lithium in $LiCoO_2$. However, the magnetic susceptibility of $LiCoO_2$ shows a weak and practically temperature independent paramagnetism, which can be attributed to Van Vleck paramagnetism for the Co^{3+} ion in a low-spin state.[34] Since the electron density is very low at the Li^+ ions, the shielding field at a given lithium spin may then be considered to arise essentially from the neighboring cobalt atoms. As in the McConnell−Pople[35,36] model used initially to calculate long-range dipolar shielding of protons, each cobalt atom may furthermore be approximated by a magnetic point dipole. With these assumptions, the expression of the resulting shift is identical to the one obtained for the paramagnetic shift due to the magnetic dipole interactions between nuclear and electron spins. Hence, the components of the shift tensor in the crystal

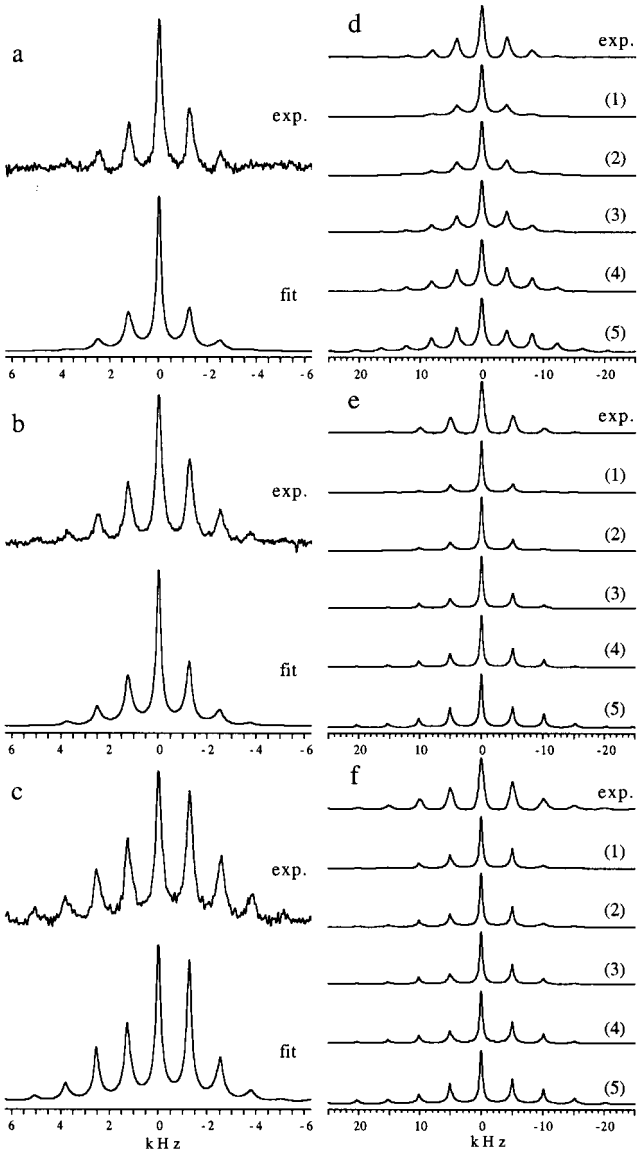

Figure 6. Experimental and fitted ^{6}Li and ^{7}Li MAS NMR spectra of $LiCoO_2$(O2) using the memory function approach (eq 1) with $\delta_S = 47 \pm 3$ ppm, $\tau_c(^6Li) = 1234 \pm 180$ μs, and $\tau_c(^7Li) = 325 \pm 100$ μs (M_2-^{6}Li $= 6.83 \times 10^7$ rad^2 s^{-2} and $M_2(^7Li) = 6.87 \times 10^8$ rad^2 s^{-2}): (a) ^{6}Li, 4.7 T, $\nu_r = 1.25$ kHz; (b) ^{6}Li, 7.1 T, $\nu_r = 1.26$ kHz; (c) ^{6}Li, 11.7 T, $\nu_r = 1.27$ kHz; (d) ^{7}Li, 4.7 T, $\nu_r = 4.10$ kHz; (e) ^{7}Li, 7.1 T, $\nu_r = 5.09$ kHz; (f) ^{7}Li, 11.7 T, $\nu_r = 5.07$ kHz; (1) $|Q_{CC}| = 0$; (2) $|Q_{CC}| = 10$ kHz; (3) $|Q_{CC}| = 20$ kHz; (4) $|Q_{CC}| = 30$ kHz; (5) $|Q_{CC}| = 40$ kHz.

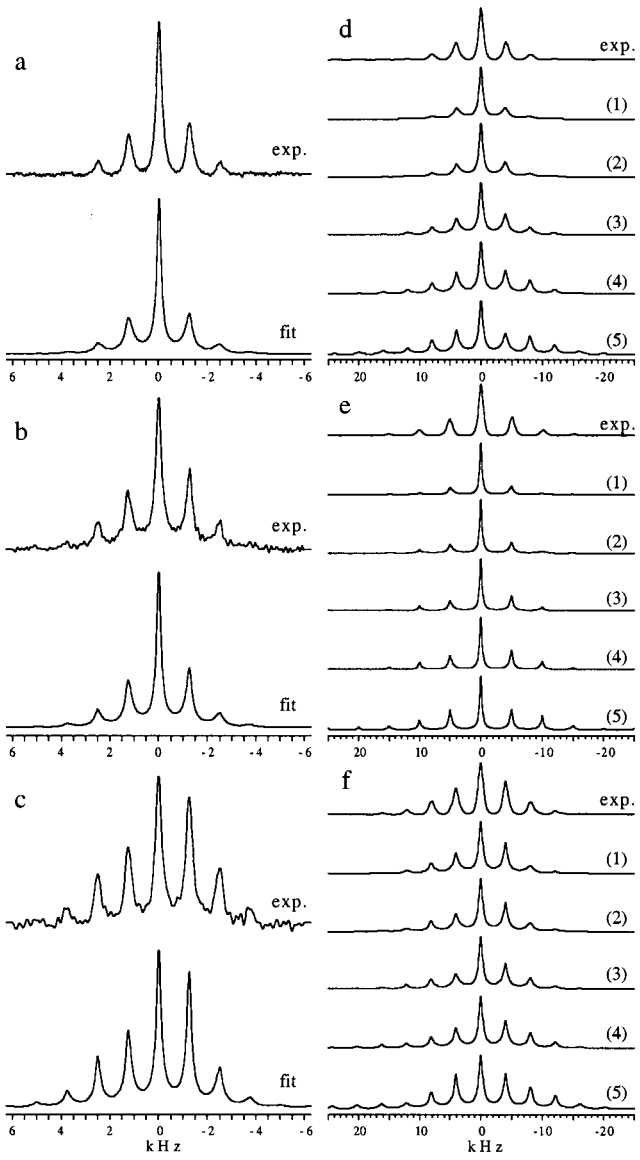

Figure 7. Experimental and fitted ^{6}Li and ^{7}Li MAS NMR spectra of $LiCoO_2$(O3) using the memory function approach (eq 1) with $\delta_S = 45 \pm 3$ ppm, $\tau_c(^6Li) = 1142 \pm 170$ μs, and $\tau_c(^7Li) = 355 \pm 80$ μs (M_2-(^{6}Li) = 6.47×10^7 rad^2 s^{-2} and $M_2(^7Li) = 6.57 \times 10^8$ rad^2 s^{-2}): (a) ^{6}Li, 4.7 T, $\nu_r = 1.25$ kHz; (b) ^{6}Li, 7.1 T, $\nu_r = 1.25$ kHz; (c) ^{6}Li, 11.7 T, $\nu_r = 1.25$ kHz; (d) ^{7}Li, 4.7 T, $\nu_r = 4.0$ kHz; (e) ^{7}Li, 7.1 T, $\nu_r = 5.0$ kHz; (f) ^{7}Li, 11.7 T, $\nu_r = 4.06$ kHz; (1) $|Q_{CC}| = 0$; (2) $|Q_{CC}| = 10$ kHz; (3) $|Q_{CC}| = 20$ kHz; (4) $|Q_{CC}| = 30$ kHz; (5) $|Q_{CC}| = 40$ kHz.

frame O*xyz* are written[37−39,18]

$$A^S_{\alpha\beta} = \frac{\chi_m}{N}\sum_i \frac{3\alpha_i\beta_i - r_i^2\delta_{\alpha\beta}}{r_i^5} \qquad (3)$$

where $\alpha,\beta = x, y, z$ ($\delta_{\alpha\beta} = 1$ if $\alpha = \beta$ and $\delta_{\alpha\beta} = 0$ otherwise) and x_i, y_i, and z_i are the coordinates of the internuclear vector $\mathbf{r}_i$ between the Li^+ reference site and the ith Co^{3+} ion. χ_m is the molar magnetic susceptibility and N is the number of Co^{3+} ions per mole of $LiCoO_2$. The direct summation over the lattice is performed numerically. We checked that the series of eq 3 has converged considering all Co^{3+} ions within a radius of 50 Å. The traceless shift tensor is subsequently diagonalized to obtain the principal components A_1^S, A_2^S, and A_3^S or, alternatively, the shift anisotropy δ_S and the asymmetry parameter η_S as well as the orientation of the **S** tensor in the crystal frame. Of course, due to the presence of a C_3 symmetry axis at the Li site in $LiCoO_2$ (O2 and O3 phases), the **S** tensor is diagonal and axially symmetric ($\eta_S = 0$) in the crystal frame, its unique principal axis lying along Oz (crystallographic axis *c*) so that $\delta_S = A_{zz}^S$. With the experimental values of χ_m at room temperature (1.03×10^{-4} cm^3/mol for the O2 phase and 1.23×10^{-4} cm^3/mol for the O3 phase), eq 3 yields shift anisotropies ($\delta_S = 47.1$ ppm for the O2 phase and $\delta_S = 46.5$ ppm for the O3 phase) in excellent agreement with the ones obtained using the memory function approach (Figures 6 and 7). This result may be taken as a clear confirmation of the fact that the magnetic susceptibility in both the O2 and O3 phases of $LiCoO_2$ is due to Van Vleck paramagnetism for Co^{3+} (LS t_2^6).

D. Point Charge Calculation of the Quadrupole Coupling Parameters. Assuming that $LiCoO_2$ crystals are predominantly ionic, we may regard the solid as an array of point charges *Ze* situated at the lattice sites (point monopole model). Note that this model has been successful in predicting the quadrupole interaction, at oxygen,[40] lithium,[18] sodium,[41] aluminum,[42] and vanadium[19] sites in various inorganic materials. The components of the EFG tensor defined as the second partial spatial derivatives of the classical electrostatic potential *V* evaluated at a given nuclear site may then be given by an expression similar to eq 3 [43]

$$A^Q_{\alpha\beta} = \frac{\partial^2 V}{\partial\alpha\partial\beta_{|\text{nucleus}}} = \frac{e}{4\pi\epsilon_0}\sum_i \zeta_i \frac{3\alpha_i\beta_i - r_i^2\delta_{\alpha\beta}}{r_i^5} \qquad (4)$$

where $e\zeta_i$ is the electric charge of the ith ion. As for the **S** tensor, due to the presence of a C_3 symmetry axis at the nuclear sites of $LiCoO_2$, the **Q** tensor is diagonal and axially symmetric ($\eta_Q = 0$) in the crystal frame ($\delta_Q = A_{zz}^Q = eq$). The calculation of the quadrupole coupling constant Q_{CC} requires also the knowledge of the Sternheimer (anti)shielding factor γ_∞, which accounts for distortions induced in the core electrons by external field gradients ($Q_{CC} = (1 - \gamma_\infty)eQ\delta_Q/h$).[43,44] The value of $(1 - \gamma_\infty) = 8$ appears to be the right magnitude for Co^{3+}.[45−47] For Li^+, γ_∞ may be considered to range from 0.25 to 0.34.[44,48] Assuming a fully ionized lithium atom ($\zeta(Li) = +1$) together with the condition of electrical neutrality, there is a linear relationship between the calculated value of Q_{CC} and the partial charge at the cobalt or at the oxygen site. Note that the partial oxygen charges of the two different oxygens (O1 and O2) in polytype O2 are assumed to be identical since the O1- and O2-cation bond lengths and, thus, bond valences[49] are equal. Figure 8 shows the variation of $Q_{CC}(^{59}Co)$ and $Q_{CC}(^7Li)$ for both polytypes O2 and O3 in the relevant range of charge values, with $\gamma_\infty(Co) = -7$ and $\gamma_\infty(Li) = 0.3$. Since only the absolute value of Q_{CC} can be determined experimentally, there are two possible solutions for the partial charges depending on the sign of the EFG. In Figure 8a, it is remarked that the partial charges derived from positive $Q_{CC}(^{59}Co)$ values are nearly identical for polytypes O2 and O3 ($\zeta(Co) = +1.855$, $\zeta(O) = -1.428$) and O3 ($\zeta(Co) = +1.864$, $\zeta(O) = -1.432$), as expected from empirical bond-valence methods[49,41] since the oxygen-cation bond lengths are practically the same in the O2 and O3 phases. The fact that the quadrupole coupling constant of phase O2 is about 3 times larger than the one of phase O3 is then almost entirely accounted for by the changes in the atomic positions (Figure 1). Moreover, Figure 8b shows that this solution leads to $|Q_{CC}(^7Li)|$ values (~40 kHz for the O2 phase and ~20 kHz for the O3 phase) in reasonable agreement with the experimental data (Figures 6 and 7). On the other hand, negative $Q_{CC}(^{59}Co)$

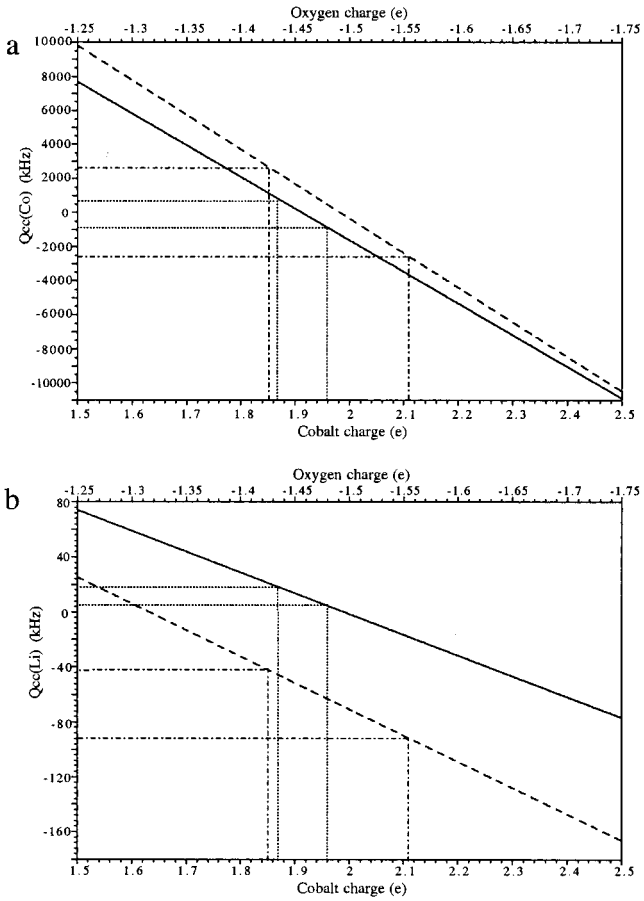

Figure 8. Variation of the quadrupole coupling constants $Q_{CC}(^{59}Co)$ (a) and $Q_{CC}(^{7}Li)$ (b) as a function of the partial charge at the cobalt site or at the oxygen site for the O2 (broken line) and O3 (solid line) phases of $LiCoO_2$. The solutions derived from the experimental $Q_{CC}(^{59}Co)$ values for the O2 and O3 phases are indicated.

values may be excluded since the deduced partial charges corresponding to the two phases then differ significantly ($\zeta(Co) = +1.96$ and $+2.11$) and lead to $|Q_{CC}(^{7}Li)|$ values ($\sim$90 kHz for the O2 phase and $\sim$5 kHz for the O3 phase) that contradict the experimental data. Hence, it is concluded that our analysis indirectly permits the determination of the sign of Q_{CC}. Finally, note that these results show that $LiCoO_2$ is significantly less ionic than expected from a simple semiempirical model such as the one introduced by Brown and coworkers,[49] which yields $\zeta(O) = -1.71$ for both polytypes O2 and O3.

E. Ab Initio Calculation of the Quadrupole Coupling Parameters. The values obtained above for the point charges of the Li, Co, and O atoms, which are, respectively $+1$, $+1.86$, and -1.43, suggest that some degree of covalency must exist between Co and O. This is somewhat in contradiction with the very hypothesis that grounds the calculation, since a significant amount of electrons must be present between Co and O and, therefore, can hardly be accounted for by considering only point charges at the atomic sites.

We therefore made an attempt to obtain the EFG parameters from first principles by taking into account the electron distribution as it results from full crystal density functional theory (DFT), using the WIEN97 package[50] to perform full-potential linearized augmented plane wave (FP-LAPW) calculations of the electronic structure. The calculations are fully ab initio in their input of neutral species at the crystal coordinates. However, these atoms are within atomic spheres with non unique muffin tin radii (R_{MT}), the remaining space being the empty interatomic space. This is involved by the energy cutoff criterion ($R_{MT}K_{max}$), as discussed below.

TABLE 3: Theoretical $|Q_{CC}|$ Values Obtained by FP-LAPW Calculations on the Two $LiCoO_2$ Phases[a]

		phase O2		phase O3	
	atomic radius (au)	$\lvert Q_{CC}(^{59}Co)\rvert$ (kHz)	$\lvert Q_{CC}(^{7}Li)\rvert$ (kHz)	$\lvert Q_{CC}(^{59}Co)\rvert$ (kHz)	$\lvert Q_{CC}(^{7}Li)\rvert$ (kHz)
Co	1.7	13 000	3.1	2 310	14.6
O	1.9				
Li	1.6				
Co	1.65	13 953	12.5	275	11
O	1.65				
Li	1.65				

[a] 100 k-points have been utilized, and $R_{MT}K_{max} = 7$. Calculations yield the $A_3^{\mathbf{Q}}$ EFG value for each nucleus. $\mathbf{Q}_{CC}$ values are calculated using eq 5.

Atomic coordinates were taken from the Rietveld refinement performed on the two materials at 300 K. Cell parameters and ionic positions were not relaxed before the calculations. The exchange and correlation potentials used was that of Ceperley and Alder[51] (in the Generalized Gradient Approximation). The E_{cutoff} convergence criterion ($R_{MT}K_{max}$) for these LAPW expansions range from 6.75 to 8. The irreducible wedge of the Brillouin zone was sampled with up to 100 k-points. Total energy was shown to be self-consistent within 0.0001 Ryd for three consecutive iterations. The quadrupole coupling constant (Q_{CC}) theoretical value is obtained from the $A_3^{\mathbf{Q}}$ ($= eq$) principal component of the EFG tensor according to the following equation:

$$Q_{CC}(\text{kHz}) = \frac{eQ}{h}(\text{kHz V}^{-1}\text{ m}^2)A_3^{\mathbf{Q}}(\text{V m}^{-2}) \qquad (5)$$

Note that there is no need for incorporating the Sternheimer factor, since all the electrons are (in principle) taken into account in a DFT-based calculation (all-electron calculation).

Such calculations proved to be rather delicate as the obtained EFG values are very sensitive to different parameters used to run the calculations. For example, the number of k-points used influences strongly the magnitude of the $A_3^{\mathbf{Q}}$ values. Calculations made with 50 k-points gave values approximately twice as high as those obtained with 100 k-points, whereas additional calculations with up to 150 k-points showed no qualitative differences. The energy cutoff criterion ($R_{MT}K_{max}$) and the atomic radius chosen for the calculations also influence the results in large proportions. Calculations made with $R_{MT}K_{max} = 6.75$ instead of 7 yielded a negative quadrupolar constant for Co in $LiCoO_2$(O3). However, the Li EFG value seems to be less sensitive to these parameters than that of Co. Table 3 shows the computed results obtained for the two varieties of $LiCoO_2$, with an energy cutoff ($R_{MT}K_{max}$) of 7 and 100 k-points (parameters for which the total energy is lowest). Different atomic radii have been used for the calculations.

The quadrupole coupling constant obtained for Co is positive for the two systems, whereas the Q_{CC} value for Li ions is positive for the O3 variety and negative for the O2 one, in agreement with the point charge calculations presented in section III.D (Figure 8). However, the computed values differ from the experimental ones, in particularly for the O2 phases, for which the Co EFG values are much too large. Nevertheless, the Co EFG values obtained for the O2 phase are larger than those obtained for the O3 one, such a trend being in agreement with the experimental observation and with the different cobalt environments.

Such EFG calculations are therefore extremely sensitive to the various parameters chosen, which makes the comparison of experimental NMR and calculated EFG data for any given material a task beyond what can be reasonably achieved in the present state of the art. They seem, however, to be appropriate for the discrimination of two signals due to a nucleus in two different sites in a same given material, since the same parameters hold for the two EFG calculations.[52]

IV. Conclusion

^{59}Co, ^{6}Li, and ^{7}Li MAS NMR combined with shift and EFG calculations is very useful for studying the structure of polytypes O2 and O3 of $LiCoO_2$. The fits of ^{59}Co NMR spectra clearly show the presence of structural disorder in $LiCoO_2$(O3), even though single cobalt and lithium resonances are observed. This fact may be tentatively related to a small departure from stoichiometry.[14] As in our previous studies,[18,53] the two lithium isotopes are shown to complement each other very well, provided that the ^{6,7}Li$-^{6,7}$Li and ^{6,7}Li$-^{59}$Co nuclear dipolar interactions are taken into account. This has been conveniently done by using a memory function approach. In this respect, it should be pointed out that iterative fitting of the line shapes at three different magnetic field strengths is mandatory for a proper evaluation of the multiple interactions acting on the ^{6}Li and ^{7}Li nuclei in $LiCoO_2$, as well as for an accurate determination of the ^{59}Co NMR interaction parameters.

The calculation of the shift coupling parameters shows that the magnetic susceptibility in both the O2 and O3 phases of $LiCoO_2$ is due to Van Vleck paramagnetism for Co^{3+} (LS t_2^6). Moreover, assuming a purely ionic lithium atom ($\zeta(Li) = +1$), the calculation of the quadrupole coupling parameters leads to identical atomic charges for phases O2 and O3 of $LiCoO_2$ ($\zeta(Co) = +1.86$ and $\zeta(O) = -1.43$). This fact clearly demonstrates that the nature of chemical bonds is very similar in these two polytypes. The magnitude of the EFG at the Cobalt site (Q_{CC} value) is nearly 3 times as large for the O2 variety as for the O3 one, which obviously results from the fact that the CoO_6 octahedra share one face and three edges with the LiO_6 octahedra in the former and six edges in the latter. Note also that the oxygen charge is close to values previously obtained[18,19] for the bridging oxygens in γ-LiV_2O_5, which are coordinated to three transition metal atoms, as in $LiCoO_2$. Analysis of such charge values in terms chemical bonds is not straightforward, since purely ionic states (point charges at the atomic sites) are assumed for the calculation, and the results suggest a significant covalency between Co and O. However, our DFT (FP-LAPW) ab initio calculations in the O2 and O3 varieties were only partially successful for obtaining such a sensitive quantity as the EFG.

Acknowledgment. We are indebted to Dr. B. Meurer of the Institut Charles Sadron, Strasbourg, France, for permitting the use of the Bruker ASX-200 spectrometer. We are also grateful to the Région Alsace for its participation in the purchase of the Bruker MSL-300 and Avance DSX-500 spectrometers. We finally thank Maurizio Mattesini for helpful discussions.

References and Notes

(1) Mizushima, K.; Jones, P. C.; Wiseman, P. J.; Goodenough, J. B. *Mater. Res. Bull.* **1980**, *15*, 783.
(2) Delmas, C.; Braconnier, J. J.; Hagenmuller, P. *Mater. Res. Bull.* **1982**, *17*, 117.
(3) Mendiboure, A.; Delmas, C.; Hagenmuller, P. *Mater. Res. Bull.* **1984**, *19*, 1383.
(4) Paulsen, J. M.; Muller-Neuhaus, J. R.; Dahn, J. R. *J. Electrochem. Soc.* **2000**, *147*, 508.
(5) Reimers, J. N.; Dahn, J. R. *J. Electrochem. Soc.* **1992**, *139*, 2091.
(6) In *Solid State NMR I-IV*; Blümich, B., Kosfeld, S., Eds.; Springer: Berlin, 1994; Vol. 30−33.
(7) Garcia, B.; Barboux, P.; Ribot, F.; Kahn-Harari, A.; Mazerolles, L.; Baffier, N. *Solid State Ionics* **1995**, *80*, 111.
(8) Ouyang, B.; Cao, X.; Lin, H. W.; Slane, S.; Kostov, S.; denBoer, M.; Greenbaum, S. G. *Mater. Res. Symp. Proc.* **1995**, *369*, 59.
(9) Carewska, M.; Scaccia, S.; Croce, F.; Arumugam, S.; Wang, Y.; Greenbaum, S. *Solid State Ionics* **1997**, *93*, 227.
(10) Ganguly, P.; Venkatraman, T. N.; Rajamohanan, P. R.; Ganapathy, S. *J. Phys. Chem. B* **1997**, *101*, 11099.
(11) Peeters, M. P. J.; Bommel, M. J. v.; Neilen-ten Wolde, P. M. C.; van Hal, H. A. M.; Keur, W. C.; Kentgens, A. P. M. *Solid State Ionics* **1998**, *112*, 41.
(12) Ménétrier, M.; Saadoune, I.; Levasseur, S.; Delmas, C. *J. Mater. Chem.* **1999**, *9*, 1135.
(13) Imanishi, N.; Fujiyoshi, M.; Takeda, Y.; Yamamoto, O.; Tabuchi, M. *Solid State Ionics* **1999**, *118*, 121.
(14) Levasseur, S.; Ménétrier, M.; Suard, E.; Delmas, C. *Solid State Ionics* **2000**, *128*, 11.
(15) Eaton, D. R.; Buist, R. J.; Sayer, B. G. *Can. J. Chem.* **1987**, *65*, 1332.
(16) Chung, S. C.; Chan, J. C. C.; Au-Yeung, S. C. F.; Xu, X. *J. Phys. Chem.* **1993**, *97*, 12685.
(17) Hirschinger, J.; Granger, P.; Rosé, J. *J. Phys. Chem.* **1992**, *96*, 4815.
(18) Hirschinger, J.; Mongrelet, T.; Marichal, C.; Granger, P.; Savariault, J. M.; Déramond, E.; Galy, J. *J. Phys. Chem.* **1993**, *97*, 10301.
(19) Marichal, C.; Kempf, J. Y.; Maigret, B.; Hirschinger, J. *Solid State Nucl. Magn. Reson.* **1997**, *8*, 33.
(20) Powell, M. J. D. *Comput. J.* **1965**, *7*, 303.
(21) Press: W. H.; Flannery, B. P.; Teukolsky, S. A.; Vetterling, W. T. *Numerical Recipes*; Cambridge University Press: Cambridge, 1986.
(22) Skibsted, J.; Nielsen, N. C.; Bildsoe, H.; Jakobsen, H. J. *Chem. Phys. Lett.* **1992**, *188*, 405.
(23) Skibsted, J.; Nielsen, N. C.; Bildsoe, H.; Jakobsen, H. J. *J. Magn. Reson.* **1991**, *95*, 88.
(24) Kempgens, P.; Harris, R. K.; Thompson, D. P. *Solid State Nucl. Magn. Reson.* **1999**, *15*, 109.
(25) Hafner, S.; Spiess, H. W. *Concepts Magn. Reson.* **1998**, *10*, 99.
(26) Abragam, A. *The Principles of Nuclear Magnetism*; Oxford University Press: Oxford, 1961.
(27) Maricq, M. M.; Waugh, J. S. *J. Chem. Phys.* **1979**, *70*, 3300.
(28) Filip, C.; Hafner, S.; Schnell, I.; Demco, D. E.; Spiess, H. W. *J. Chem. Phys.* **1999**, *110*, 423.
(29) Mehring, M. *Principles of High Resolution NMR in Solids*; Springer: Berlin, 1983.
(30) Kessemeier, H.; Norberg, R. E. *Phys. Rev.* **1967**, *155*, 321.
(31) Engelke, F.; Kind, T.; Michel, D.; Pruski, M.; Gerstein, B. C. *J. Magn. Reson.* **1991**, *95*, 286.
(32) Reinheimer, P.; Hirschinger, J.; Gilard, P.; Goetz, N. *Magn. Reson. Chem.* **1997**, *35*, 757.
(33) Anderson, P. W.; Weiss, P. R. *Rev. Mod. Phys.* **1953**, *25*, 269.
(34) Kikkawa, S.; Miyazaki, S.; Koizumi, M. *J. Solid State Chem.* **1986**, *62*, 35.
(35) McConnell, H. M. *J. Chem. Phys.* **1957**, *27*, 226.
(36) Pople, J. A. *J. Chem. Phys.* **1956**, *24*, 1111.
(37) Shulman, R. G.; Jaccarino, V. *Phys. Rev.* **1957**, *108*, 1219.
(38) Shulman, R. G.; Knox, K. *Phys. Rev.* **1960**, *119*, 94.
(39) Bleaney, B. *Phys. Rev.* **1956**, *104*, 1190.
(40) Walter, T. H.; Oldfield, E. *J. Phys. Chem.* **1989**, *93*, 6744.
(41) Koller, H.; Engelhardt, G.; Kentgens, A. P. M.; Sauer, J. *J. Phys. Chem.* **1994**, *98*, 1544.
(42) Dirken, P. J.; Nachtegaal, G. H.; Kentgens, A. P. M. *Solid State Nucl. Magn. Reson.* **1995**, *5*, 189.
(43) Cohen, M. H.; Reif, F. In *Solid State Physics, Advances in Research and Applications*; Seitz, F., Turnbull, D., Eds.; Academic Press: New York, 1957; Vol. 5, p 321.
(44) Lucken, E. A. C. *Nuclear Quadrupole Coupling Constants*; Academic Press: London, 1969.
(45) Scott, B. A.; Bernheim, R. A. *J. Chem. Phys.* **1966**, *44*, 2004.
(46) Brill, T. B.; Hugus, Z. Z. *J. Phys. Chem.* **1970**, *74*, 3022.
(47) Brown, T. L. *Accounts Chem. Res.* **1974**, *7*, 408.
(48) Lahiri, J.; Mukherji, A. *Proc. Phys. Soc.* **1966**, *87*, 913.
(49) Brown, I. D.; Altermatt, D. *Acta Crystallogr.* **1985**, *B41*, 244.
(50) Blaha, P.; Schwarz, K.; Dufek, P.; Augustyn, R. *WIEN97, Technical University of Vienna* 1997. (Improved and updated Unix version of the original copyrighted WIEN-code, which was published by P. Blaha, K. Schwarz, P. Sorantin, and S. B. Trickey in *Comput. Phys. Commun.* **1990**, *59*, 399.)
(51) Ceperley, D. M.; Alder, B. J. *Phys. Rev. Lett.* **1980**, *45*, 566.
(52) Bryant, P. L.; Harwell, C. R.; Wu, K.; Fronczek, F. R.; Hall, R. W.; Butler, L. G. *J. Phys. Chem. A* **1999**, *103*, 5246.
(53) Marichal, C.; Hirschinger, J.; Granger, P.; Ménétrier, M.; Rougier, A.; Delmas, C. *Inorg. Chem.* **1995**, *34*, 1773.